



Turning fluorescent silica nanoparticles for the removal and detection of 4-nitrophenol

Tien Thi My Le^{1,2} · Ngoc Xuan Dat Mai^{1,2} · Hanh Kieu Thi Ta^{1,2,3} · Tan Le Hoang Doan^{1,2} · Linh Ho Thuy Nguyen^{1,2}

Accepted: 2 October 2022 / Published online: 30 October 2022

© The Author(s), under exclusive licence to Springer Science+Business Media, LLC, part of Springer Nature 2022

Abstract

4-Nitrophenol (4-NP) is a dangerous compound that can be found in insecticides and pesticides in agriculture. Therefore, removing and detecting this compound in water sources are essential for the ecosystem and human health. In this study, we synthesized fluorescence-incorporated mesoporous nano silica (F-NS) for the removal and detection of 4-NP. The fluorescent nanomaterial was characterized by techniques, including Fourier-transform infrared spectroscopy, thermal gravimetric analysis, nitrogen adsorption isotherms, and scanning electron microscope. The isotherm and kinetics investigation showed that 4-NP adsorption of the nanomaterial with high capacity (up to 0.7 mg mg^{-1}) was well fitted with the multilayer adsorption and the pseudo-second-order model. Furthermore, modulation of the fluorescein isothiocyanate amount on the nanomaterial allowed the detection of 4-NP at low concentrations through fluorescence quenching.

Keywords Mesoporous silica nanoparticles · Fluorescein isothiocyanate · 4-nitrophenol · Detection · Removal

1 Introduction

Phenols are essential compounds in synthesizing drugs, insecticides, and food dyes [1–9]. 4-Nitrophenol or *p*-nitrophenol (4-NP) is one of the most harmful phenol compounds that potentially causes kidney and liver damage, cyanosis, confusion, and unconsciousness [1, 2]. Furthermore, wastewater generated from industries containing this compound could cause enhanced toxicity in groundwater [3–7]. Therefore, many approaches such as membrane filtration, adsorption, and catalytic reduction have been developed for 4-NP treatment [8–10]. Because of, using adsorbents such as carbon nanotube, montmorillonite, polymer-supported ion liquid, porous organic polymer, and mesoporous silica is an efficient method to remove 4-NP [11–16].

Besides the treatment of 4-NP, detection of its presence in solution is important. Therefore, synthesizing and exploring new materials to detect 4-NP with high accuracy and sensitivity are highly desired. Among them, the materials containing fluorescent agents have gained much attention to detect 4-NP with simple sample preparation procedures, higher sensitivity, and competitive cost [17]. 4-NP could be detected through electron transfer and fluorescence quenching mechanism [18] by fluorescent materials such as polymer carbon dot optical (PCD) [19, 20], quantum dot molecular imprinting polymer QD@MIPs [21], coumarin-based molecular imprinted polymer [22], bovine serum albumin functionalized fluorescent gold nanoclusters (BSA Au-NCs) [23], carbon quantum dots-immobilized zirconium-based metal-organic framework (CQDs@UiO-66) [24], dual-emissive gold nanoclusters [25], and mesoporous silica fluorescent sensor [26].

Mesoporous silica nanoparticles have been widely used in various applications due to their high stability and tunable structure [27–30]. The robust structure and large pores of the nano-silica materials are highly conducive to the diffusion of liquid molecules onto the adsorbent or the catalyst activity for the treatment of phenolic contaminants [31–39]. These nanoparticles could be reduced their particle sizes or modified functional groups on mesoporous silica, allowing for the development of the fluorescent sensor or biomedical

✉ Tan Le Hoang Doan
dlhtan@inomar.edu.vn

✉ Linh Ho Thuy Nguyen
nhtlinh@inomar.edu.vn

¹ Center for Innovative Materials and Architectures,
Ho Chi Minh City, Vietnam

² Vietnam National University-Ho Chi Minh City,
Ho Chi Minh City, Vietnam

³ Faculty of Materials Science and Technology, University
of Science, Ho Chi Minh City, Vietnam

application [8, 27, 40]. In addition, the nanoparticles are low toxicity and high reactivity with polymers or fluorescent compounds [41–43] to enhance 4-NP detection [44, 45].

In this study, fluorescein isothiocyanate (FITC) was chosen as a marker compound to make F-NS materials and detect 4-NP via quench fluorescence signal. We screened the molar ratios of FITC to tetraethyl orthosilicate (TEOS) in the synthesis of F-NS (named MFA 1, MFA 2, MFA 3, and MFA 4). Liquid adsorption and fluorescence quenching evaluated the removal and detection of 4-nitrophenol. The remarkable removal of 4-NP is over 90% by F-NS and determined by the UV-VIS method with encapsulation efficiencies up to 0.7 mg mg^{-1} . Furthermore, the removal of 4-NP was investigated through the isotherm, kinetic study, and fluorescence quenching.

2 Experiment

2.1 Reagents and chemicals

Tetraethyl orthosilicate and cetyltrimethylammonium bromide (CTAB) were purchased from Acros. 3-Aminopropyltriethoxysilane (APTES) and fluorescein isothiocyanate were obtained from Sigma Aldrich. 4-nitrophenol (4-NP), hydrochloric acid (HCl), ethanol (EtOH), and acetonitrile (AcCN) were bought from Fisher.

2.2 General method

Fourier transform infrared (FT-IR) spectra were collected in the region of $4000\text{--}400 \text{ cm}^{-1}$ on a Bruker Vertex 70 spectrometer using KBr tablets. Thermogravimetric analysis (TGA) was measured on a TA Instruments Q500 under continuous airflow with a temperature increase of $5 \text{ }^\circ\text{C}/\text{min}$ from room temperature to $800 \text{ }^\circ\text{C}$. The Quantachrome Autosorb iQ2 analyzer measured low-pressure N_2 adsorption isotherms at 77 K . Field emission scanning electron images were captured with FE-SEM (Japan, Hitachi, S4800). UV-Vis spectra of 4-NP were recorded on a JASCO V-670 spectrophotometer. Material images were taken on Olympus BX-53 to observe the fluorescence signals.

2.3 Materials synthesis

2.3.1 Synthesis of MCM-41

A mixture of 120 mL deionized (DI) water and 1.75 mL NaOH 1 M were added in a round bottom flask with a mass of 250 mg CTAB. This solution was stirred at 1500 rpm at $80 \text{ }^\circ\text{C}$ until the stability system, a volume of 1.25 mL TEOS (5.59 mmol), was added in the flask and kept stirring at $80 \text{ }^\circ\text{C}$ for 2 h. The mixture was centrifugated to collect solid and was washed

with 50 mL ethanol two times. The CTAB surfactants were removed by dispersing the as-synthesized material in ethanol (60 mL) and concentrated HCl (1.0 mL), and refluxed for 8 h. The material was collected by centrifugation, washed with ethanol, and dried under vacuum at $80 \text{ }^\circ\text{C}$ for 8 h.

2.3.2 Synthesis of FITC@mesoporous silica nanoparticles (F-NS)

The incorporation of FITC on MCM-41 structure was synthesized based on our previous report with slight modifications [46]. Four FITC solutions namely FA 1, FA 2, FA 3, and FA 4 were prepared in a volume of 5 mL ethanol and stirred gently for 30 min in the dark with FITC/TEOS mole ratios of 0.22×10^{-3} , 0.45×10^{-3} , 0.56×10^{-3} , and 1.13×10^{-3} , respectively. At the same time, a volume of 960 mL DI water and 14 mL NaOH 1 M were evenly poured into four round bottom flasks with a mass of 500 mg CTAB for each and stirred at $80 \text{ }^\circ\text{C}$. After that, The FITC solutions were added to these flasks and kept stirring at $80 \text{ }^\circ\text{C}$ for 2 h. The solid samples were centrifugated by centrifugation and washed twice with 48 mL ethanol. CTAB was removed from materials via the reflux in a mixture of 2 mL hydrochloric acid and 100 mL ethanol at $80 \text{ }^\circ\text{C}$ for 8 h. F-NS samples were collected by centrifugation at 16,000 rpm for 5 min and washed two times with ethanol and DI H_2O . The activated F-NS samples were dried under a high vacuum at $120 \text{ }^\circ\text{C}$ for 12 h.

2.3.3 Procedure for 4-nitrophenol adsorption

Stock solution (5000 mg L^{-1}) of 4-NP was obtained by dissolving in acetonitrile, and the low concentrations of 4-NP from 139 to 3475 mg L^{-1} were diluted via adding solvent to the stock solution. The 4-NP adsorption process was investigated based on the concentrations of 4-NP, adsorption time, and the different materials such as MCM-41 and F-NS. 1.5 mL of the accurate 4-NP concentrations was immersed with 5 mg of material at $37 \text{ }^\circ\text{C}$ for 120 min. After that, the adsorbents were collected by centrifugation at 16,000 rpm for 30 min to observe under a fluorescent microscope. The calibration curve of 4-NP between concentration and absorbance was measured with the UV-VIS spectrophotometer at a wavelength of 310 nm. The 4-NP solutions were recorded from the UV-VIS spectra and calculated from the calibration curve equation.

3 Results and discussion

3.1 Characterization of nanoparticle properties and structures

TEOS and CTAB were essential ingredients and agents to create the mesoporous nanoparticles, while FITC and

APTES were fluorophores to detect 4-NP. F-NS materials were determined by FT-IR, TGA, N_2 sorption isotherms, and fluorescence microscope to investigate the properties and structure of the materials.

FT-IR spectra of MCM-41, MFA 1, MFA 2, MFA 3, and MFA 4 were performed in the region of $4000-400\text{ cm}^{-1}$. Figure 1a showed the signal of Si-O-Si bonds at 1060 cm^{-1} , Si-OH bonds at 960 cm^{-1} , and C-S bonds at $667-694\text{ cm}^{-1}$, respectively, matching the literature [47]. The new bands, at 3217 cm^{-1} and 2928 cm^{-1} , derived from N-H stretching and an aromatic secondary amine group (-NH), determined the presence of FITC and APTES in F-NS materials [48]. Besides, there was not stretching vibration of aliphatic C-H at 3000 cm^{-1} , indicating that CTAB was entirely removed by washing in ethanol and deionized water.

F-NS materials were measured by thermogravimetric analysis (TGA) under airflow from room temperature to $800\text{ }^\circ\text{C}$. Based on the TGA diagram (Fig. 1b) showed the mass change of the material over two temperature periods. Below $300\text{ }^\circ\text{C}$, the mass loss of F-NS materials was about 10%, corresponding to the burning of organic molecules such as FITC and APTES. The small weight change of the F-NS materials was consistent with the small amount of grafted FITC and APTES on MCM-41.

The nitrogen adsorption-desorption isotherm of MCM-41 and F-NS materials was measured at 77 K (Fig. 2), corresponding to a type IV isotherm of mesoporous material [49]. According to the Brunauer-Emmett-Teller (BET), the surface areas were around $1000-1300\text{ m}^2\text{ g}^{-1}$ for MFA 1, MFA 2, MFA 3, and MFA 4 (Table 1). According to the B.J.H model, the pore diameter of F-NS materials slight decreased for samples that contained a high mole ratio of FITC/TEOS (Fig. 2). These results proved the success in synthesizing

F-NS materials via FITC/TEOS mole ratio adjustment without greatly affecting the pore space of the materials.

FE-SEM determined the morphology of the MCM-41 and F-NS powders. Figure 3 showed that materials had a spherical and ellipsoidal shape with sizes around $50-150\text{ nm}$. MCM-41 material had a particle size distribution in the range of $100-120\text{ nm}$ while the F-NS materials had a slightly reduced particle size in the range of $80-120\text{ nm}$ (Table 1 and Fig. S1). Moreover, FITC combining MCM-41 showed the morphological change from spherical to ellipsoidal. The increase in CTAB mass during the synthesis of F-NS materials could be responsible for the slight decrease in particle size and morphology of the materials. In addition, the material samples observed under the fluorescence microscope showed a gradual increase in luminescence (shown in Fig. 4), which corresponds to an increase in the amount of FITC during the preparation process.

3.2 Adsorption experiments

3.2.1 Adsorption isotherms

Calibration curve equation was built by the various concentration of 4-NP and the absorbance values from UV spectra and showed in the Fig. S2. The linear regression equation with a correlation coefficient (R^2) of approximately 1 indicated a linearity between absorbance and concentration of 4-NP. Therefore, it could be used to calculate the concentration of 4-NP in the samples after performing adsorption.

Subsequently, we employed F-NS materials to carry out the adsorption of 4-NP. The activated samples (5 mg) were added to 10 mL of 4-NP with a specific concentration for 120 min . After a certain period, the 4-NP diluted solution

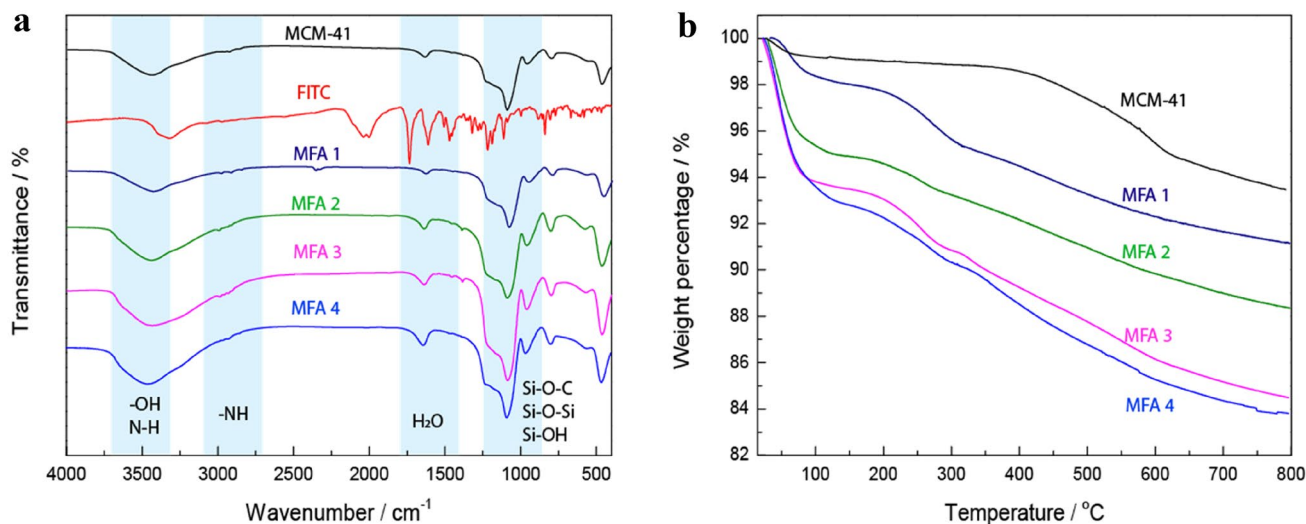


Fig. 1 **a** FT-IR spectra and **b** TGA of MCM-41 and F-NS materials

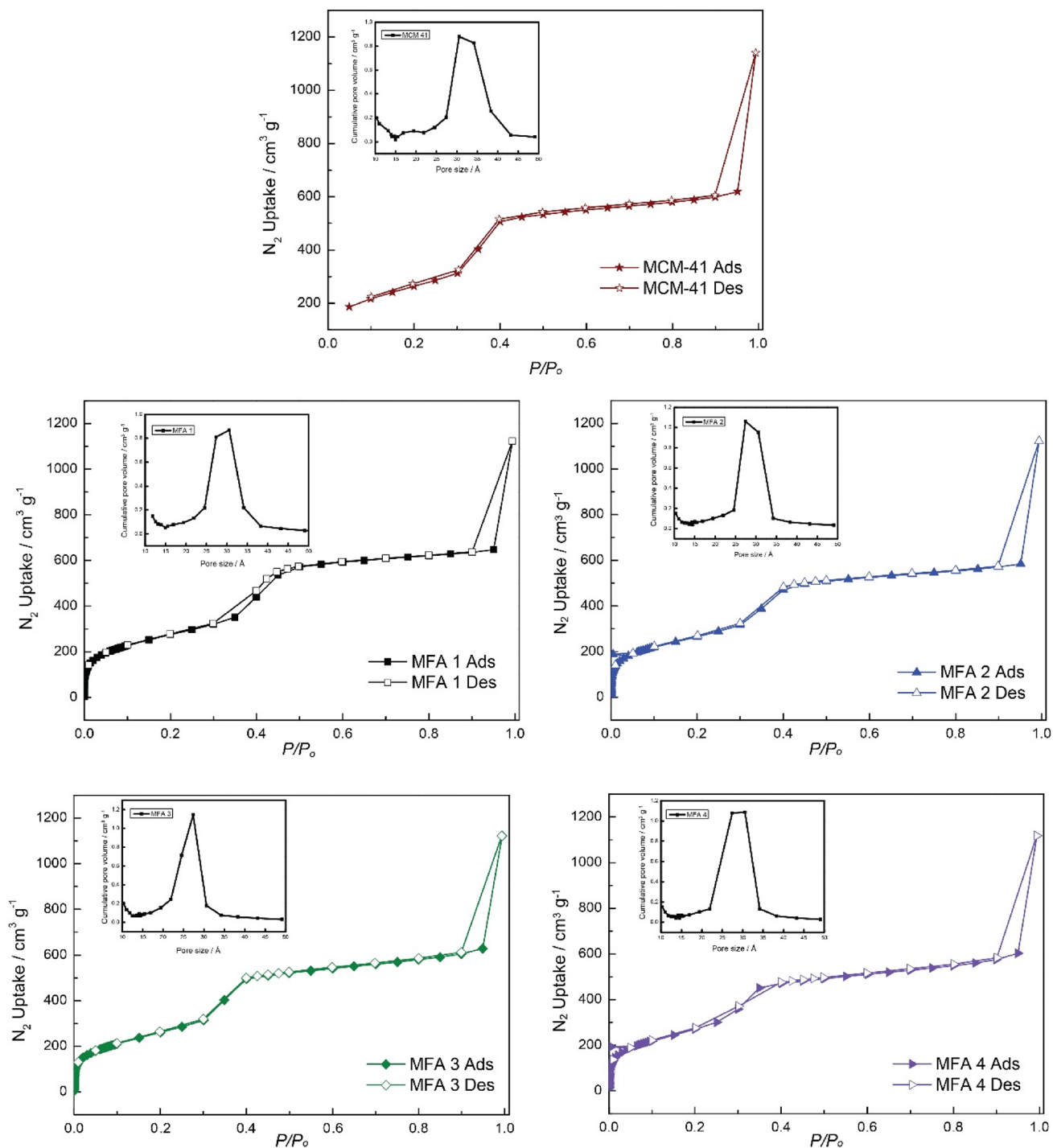


Fig. 2 Nitrogen adsorption-desorption isotherms and Pore size distribution curves of MCM-41 and F-NS materials following the Barrett-Joyner-Halenda Model (B.J.H).

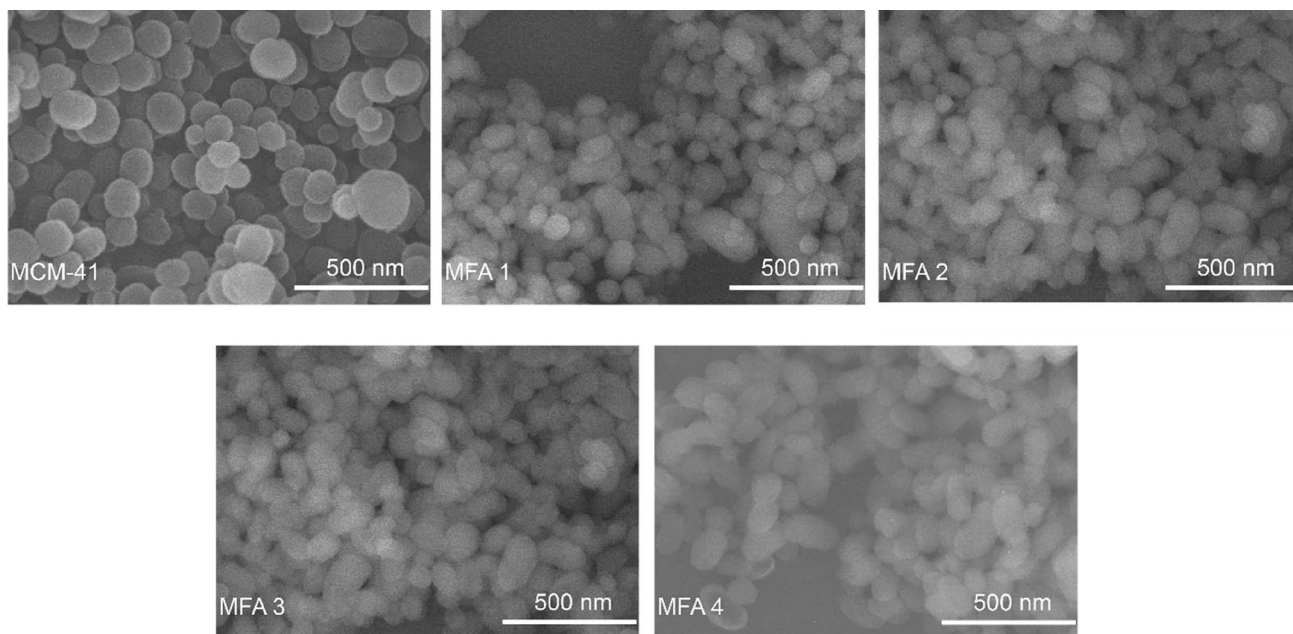


Fig. 3 SEM of MCM-41 and F-NS materials with a magnification of 100,000 times

Table 1 Textural properties of MCM-41 and F-NS materials

Entry	Materials	$S_{B,E,T}$ ($m^2 g^{-1}$)	Pore diameter (Å)	Particle size (nm)
1	MCM-41	1332	30–36	100–120
2	MFA 1	1317	25–30	80–100
3	MFA 2	1293	25–30	80–120
4	MFA 3	1075	22–30	80–120
5	MFA 4	1066	22–30	80–120

was recorded by the JASCOV V-670 spectrophotometer at wavelength of 310 nm. The loading capacity of 4-NP (q_e) was calculated by Eq. (1) [50].

$$q_e = \frac{V(C_o - C_e)}{W} (mgg^{-1}) \tag{1}$$

where the initial and equilibrium concentrations ($mg L^{-1}$) are denoted C_o and C_e , respectively. The volume of the 4-NP

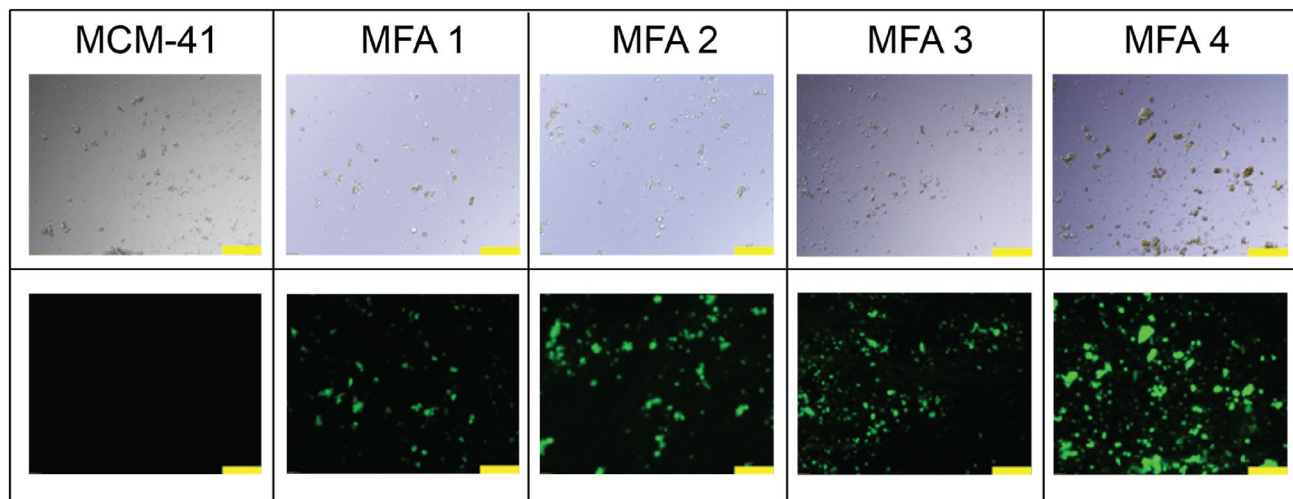


Fig. 4 Bright-field and fluorescence images of MCM-41 and F-NS materials with a scale of 100 μm

solution (mL), and the initial mass of the adsorbent (mg) are annotated as V and W .

The absorbance intensity of 4-NP at 310 nm was the lowest when using MCM-41 and increases in that of F-NS materials, which was shown in Fig. 5a. The adsorption yield of 4-NP by various materials was investigated by increasing the adsorbent dosage from 139 mg L^{-1} to 3475 mg L^{-1} , as shown in Fig. 5b. It was observed that the encapsulation of 4-NP enhanced from 0.03 to 0.7 mg mg^{-1} with increasing in 4-NP dosage. The most noteworthy 4-NP adsorption behavior of MCM-41 was attributed to the high surface area and sizeable porous diameter (see Table 1) of this material compared with F-NS materials.

The Langmuir and Freundlich models considered the monolayer and multilayer adsorption of MCM-41 and F-NS materials. As shown in Table 2, the correlation coefficient values (R^2) were more extensive than 0.99 for the Langmuir model, and the value of R_L (calculated from Eq. S2) was between 0 and 1, suggesting favorable adsorption of 4-NP onto the MCM-41 and its functional materials. However, the amount of adsorption of 4-NP at a

hypothetical saturation capacity from the Langmuir model was smaller than the loading capacity in the 4-NP experimental adsorption for two kinds of materials. The adsorption of 4-NP on these materials could occur according to the Freundlich model since the moderate value intensity (n) values (above 1) and the high R^2 values (approximately 0.99), which were collected from the linear plot of $\ln(q_e)$ versus $\ln(C_e)$. This result revealed the multilayer adsorption onto MCM-41 and F-NS materials.

The FTIR spectra of materials after loading confirmed the presence of absorbance molecules in the range of $4000\text{--}400 \text{ cm}^{-1}$, as shown in Fig. S4. The characteristic signal of 4-NP at 3250 , 1590 , and 1500 cm^{-1} was attributed to -OH stretching, $\text{C}=\text{C}$ arene, and nitro group. The FTIR spectra of F-NS materials could observe the small signals at 1590 and 1500 cm^{-1} , corresponding to the arene and nitro group of 4-NP after loading on materials. The adsorbed materials were analyzed for N_2 adsorption at 77 K to consider the change in pore space. The results in Fig. S5 showed a change in the adsorption curves with the loss of characteristic adsorption curves of the mesoporous

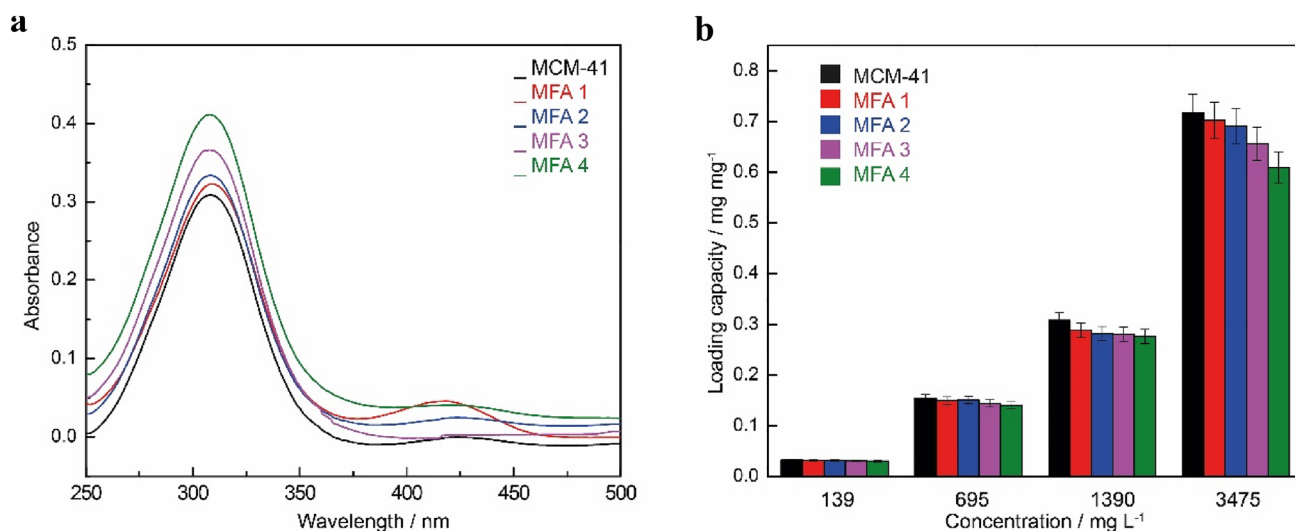


Fig. 5 **a** UV-V spectra at a concentration of 139 mg L^{-1} and **b** the loading capacity of MCM-41 and F-NS materials at concentrations of $139\text{--}3475 \text{ mg L}^{-1}$

Table 2 Estimated constants from the Langmuir and Freundlich isotherms for 4-NP adsorption by MCM-41 and F-NS materials

Entry	Materials	Langmuir			Freundlich		
		k_L (L mg^{-1})	q_s (mg g^{-1})	R^2	K_F ($\text{mg}^{1-n} \text{ L}^n \text{ g}^{-1}$)	n_F	R^2
1	MCM-41	2.093	0.476	0.994	0.378	1.383	0.995
2	MFA 1	2.469	0.392	0.999	0.329	1.428	0.993
3	MFA 2	2.479	0.388	0.997	0.314	1.463	0.994
4	MFA 3	2.724	0.339	0.997	0.278	1.498	0.991
5	MFA 4	2.871	0.304	0.980	0.237	1.635	0.992

materials. The calculated BET surface area was reduced by about 40–64% for all materials, demonstrating their high adsorption efficiency (Table 3). On the other hand, the pore diameter of materials decreased by about 16–66%, indicating the presence of 4-NP inside the pores (Table 3).

The post-adsorption material samples were collected for fluorescence microscopy observation based on the fluorescence quenching properties of FITC and 4-NP. Although the 4-NP removal efficiency increased rapidly in the early stage of the adsorption, the 4-NP adsorption equilibrium onto the MFA 1 was reached after 120 min. MFA could adsorb higher than of the other F-NS materials (Fig. 4), while its fluorescence signal was significantly reduced (Fig. 6). The small amount of FITC in MFA 1 does not significantly limit the uptake but also increase the ability to detect 4-NP. This result showed that MFA 1 has been the potential to detect 4-NP at a concentration of 139 mg L^{-1} through fluorescence quenching. Therefore, adjusting the FITC/TEOS ratios in the MCM-41 material allowed for forming materials capable of capturing and detecting 4-NP at different concentrations. In addition, MFA 4 and adsorbed MFA 4 were measured by the UV-VIS spectrophotometer. Fig. S6 showed the maximum

absorption at the light of wavelength 491 nm, related to the optical absorbance of FITC group. The decreased absorbance in the UV spectrum of adsorbed MFA 4 at the same wavelength demonstrated the interaction between MFA 4 and 4-NP.

3.2.2 Kinetic study

To observe the effect of adsorption and fluorescence quenching time, MFA 1 was used for the 4-NP adsorption experiment at an initial concentration of 139 mg L^{-1} from 30 to 120 min. The 4-NP solution was measured optical absorbance by using a UV-VIS spectrophotometer in the 250–500 nm wavelength region, as presented in Fig. 7a. It represented the absorption maximum at 310 nm, and the loading capacity of MFA 1 was increased very little over 30–120 min (Fig. 8b).

The fitting linear according to kinetic models and calculated parameters were presented in Fig. S6 and Table 4. The correlation coefficient R^2 for the pseudo-second-order was closed to 1 (Fig. S6b), and the calculated equilibrium adsorption amount (q_e) from fitting results

Table 3 Textural properties of adsorbed MCM-41 and adsorbed F-NS materials

Entry	Materials	$S_{\text{B.E.T}}$ ($\text{m}^2 \text{g}^{-1}$)	Percentage change of $S_{\text{B.E.T}}$ (%)	Pore diameter (\AA)	Percentage change of Pore diameter (%)
1	MCM-41	473	64	15–25	30–66
2	MFA 1	508	61	15–25	16–40
3	MFA 2	556	53	15–25	16–40
4	MFA 3	605	48	15–25	16–21
5	MFA 4	633	40	15–25	16–21

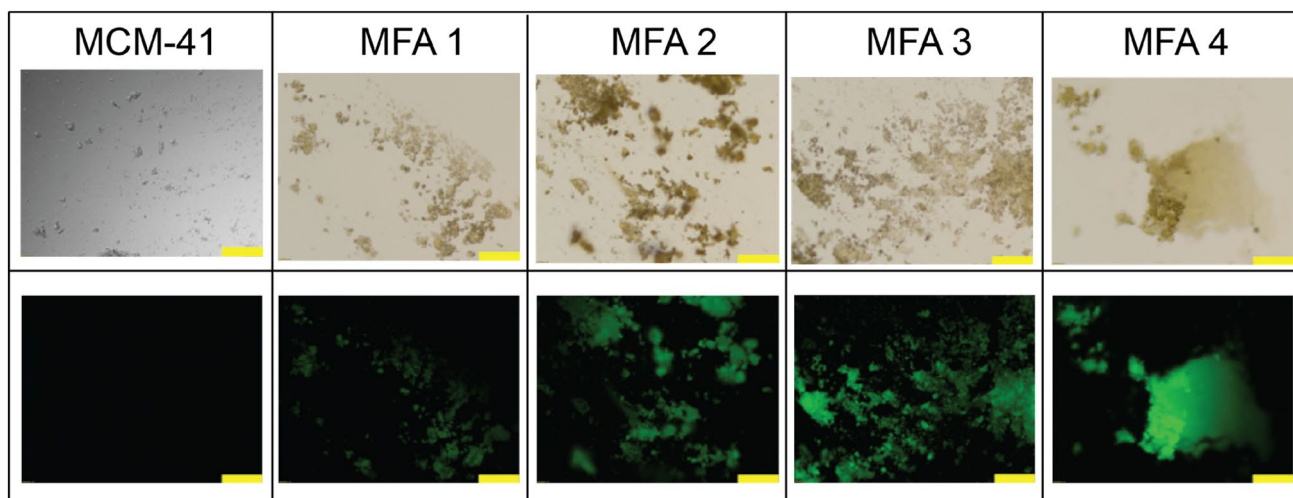


Fig. 6 Bright-field and fluorescence images of MCM-41 and F-NS materials at a 4-NP concentration of 139 mg L^{-1} for 120 min with a scale of $200 \mu\text{m}$

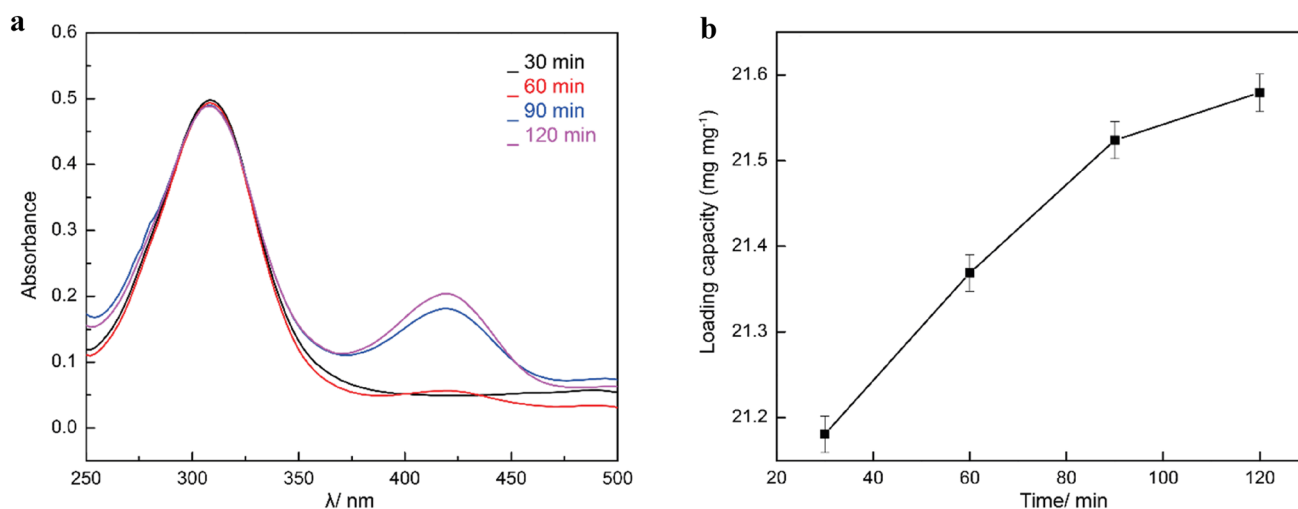


Fig. 7 UV–VIS spectra at an initial concentration of 139 mg L^{-1} and **b** the loading capacity of 4-NP adsorption over time onto MFA 1

Table 4 Kinetics parameters for the 4-NP adsorption on MFA 1 with an initial concentration of 100 mg L^{-1}

Entry	Models	q_e (exp.) mg g^{-1}	Parameters
1	<i>Pseudo-first-order</i>	31.27	k_1 (s^{-1})
2			$q_{e(\text{cal.})}$ (mg g^{-1}) R^2
3	<i>Pseudo-second-order</i>		k_2 ($\text{g mg}^{-1} \text{min}^{-1}$)
4			$q_{e(\text{cal.})}$ (mg g^{-1}) R^2

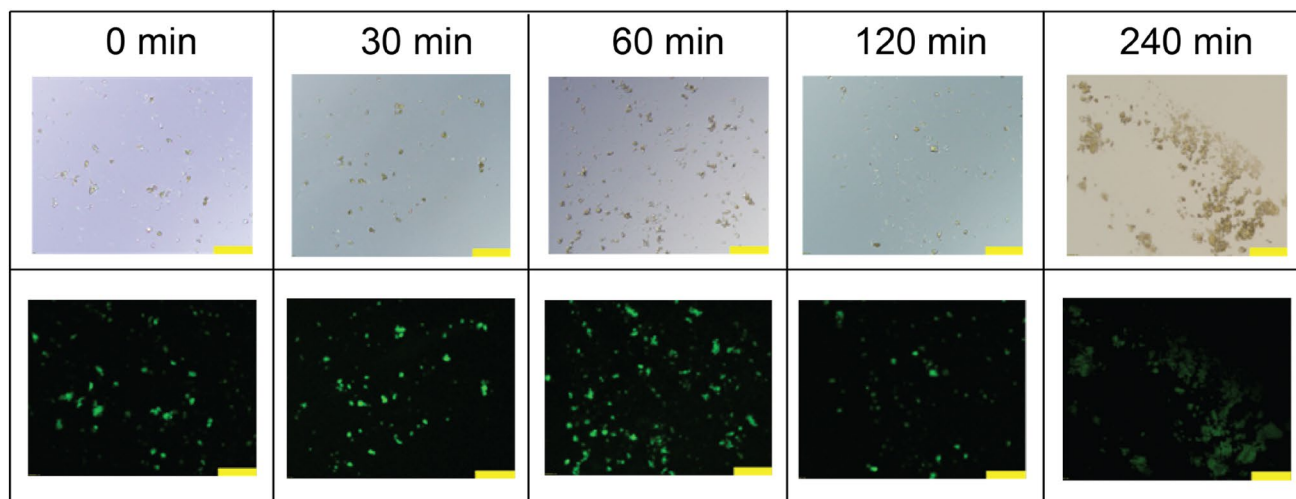


Fig. 8 Bright-field and fluorescence images of MFA 1 at an initial concentration of 139 mg L^{-1} with a scale of $200 \mu\text{m}$

was 31.24 mg g^{-1} , approaching the experimental data of 31.27 mg g^{-1} . Therefore, the kinetic model of 4-NP onto MFA 1 followed the pseudo-second-order model. Fluorescence microscopy observations revealed that a decrease in the fluorescence signal could be related to the interaction between 4-NP and MFA 1 after 120 min (Fig. 8).

According to the previous literature, we predicted that the Meisenheimer complex had been formed between the amine of APTES and carbon of 4-NP. The electron withdrawal of the nitro group supported the stabilization of the acid–base-pairing interaction. The fluorescence quenching occurred when 4-NP was combined with MFA 1 by the

resonance energy transfer between FITC and Meisenheimer complex [51].

4 Conclusion

The study provided a procedure to prepare the nanoparticles of F-NS in fluorescence customized amounts to capture and detect 4-NP compounds at a wide range of concentrations. The 4-NP sorption isotherm showed the high removal achieved approximately was 60–75% of 4-NP and followed the Freundlich isotherm model and pseudo-second-order model kinetic. The resonance energy transferred from the amine group to 4-NP after 120 min, leading to fluorescence quenching. Using fluorescence probes onto mesoporous silica was a simple approach to create the sensing material for detecting of 4-NP.

Supplementary Information The online version contains supplementary material available at <https://doi.org/10.1007/s10934-022-01364-5>.

Acknowledgements This research was supported by the Vietnam National University, Ho Chi Minh City under grant number TX2022-50-01. The authors express their sincere thanks to Applied Physical Chemistry Laboratory (APC Lab), VNUHCM-University of Science, Viet Nam for their support in using the UV-VIS spectrophotometer.

Author contributions TTML: investigation, formal analysis, writing – original draft. NXDM, HKTT: validation, resources. TLHD, LHTN: conceptualization, methodology, visualization, project administration.

Declarations

Conflict of interest The authors declare that they have no known competing financial interests or personal relationships that could have appeared to influence the work reported in this paper.

References

1. C. Yin, J. Cai, L. Gao, J. Yin, J. Zhou, Highly efficient degradation of 4-nitrophenol over the catalyst of Mn₂O₃/AC by microwave catalytic oxidation degradation method. *J. Hazard. Mater.* **305**, 15–20 (2016)
2. C. Matus, E. Camú, M. Villarroel, J. Ojeda, P. Baeza, Study of the removal of 4-nitrophenol from aqueous media by adsorption on different materials. *J. Chil. Chem. Soc.* **61**, 2898–2902 (2016)
3. X. Sun, Y. Wang, Y. Lei, Fluorescence based explosive detection: from mechanisms to sensory materials. *Chem. Soc. Rev.* **44**(22), 8019–8061 (2015)
4. Y.J. Diaz, Z.A. Page, A.S. Knight, N.J. Treat, J.R. Hemmer, C.J. Hawker, J. Read de Alaniz, A versatile and highly selective colorimetric sensor for the detection of amines, chemistry *Eur. J.* **23**(15), 3562–3566 (2017)
5. S. Kubendhiran, R. Sakthivel, S.-M. Chen, B. Mutharani, T.-W. Chen, Innovative strategy based on a novel carbon-black – β -cyclodextrin nanocomposite for the simultaneous determination of the anticancer drug flutamide and the environmental pollutant 4-nitrophenol. *Anal. Chem.* **90**(10), 6283–6291 (2018)
6. Y. Lu, X. Wan, L. Li, P. Sun, G. Liu, Synthesis of a reusable composite of graphene and silver nanoparticles for catalytic reduction of 4-nitrophenol and performance as anti-colorectal carcinoma. *J. Mater. Res. Technol.* **12**, 1832–1843 (2021)
7. X. Kong, Z. Sun, M. Chen, C. Chen, Q. Chen, Metal-free catalytic reduction of 4-nitrophenol to 4-aminophenol by N-doped graphene. *Energy Environ. Sci.* **6**(11), 3260–3266 (2013)
8. F.M.M. Tchieno, I.K. Tonle, p-Nitrophenol determination and remediation: an overview. *Rev. Anal. Chem.* (2018). <https://doi.org/10.1515/revac-2017-0019>
9. A.A. Yahya, K.T. Rashid, M.Y. Ghadhbhan, N.E. Mousa, H.S. Majdi, I.K. Salih, Q.F. Alsahly, Removal of 4-nitrophenol from aqueous solution by using polyphenylsulfone-based blend membranes: characterization and performance. *Membranes* **11**(3), 171 (2021)
10. J.N. Appaturi, T. Pulingam, S. Muniandy, I.J. Dinshaw, L.B. Fen, M.R. Johan, Supported cobalt nanoparticles on graphene oxide/mesoporous silica for oxidation of phenol and electrochemical detection of H₂O₂ and Salmonella spp. *Mater. Chem. Phys.* **232**, 493–505 (2019)
11. Y.-X. Yao, H.-B. Li, J.-Y. Liu, X.-L. Tan, J.-G. Yu, Z.-G. Peng, Removal and adsorption of p-nitrophenol from aqueous solutions using carbon nanotubes and their composites. *J. Nanomater.* **2014**, 571745 (2014)
12. M.El Ouardi, M. Laabd, H. Abou Oualid, Y. Brahmi, A. Abaamrane, A. Elouahli, A. Ait Addi, A. Laknifi, Efficient removal of p-nitrophenol from water using montmorillonite clay: insights into the adsorption mechanism, process optimization, and regeneration. *Environ. Sci. Pollut. Res.* **26**(19), 19615–19631 (2019)
13. I. Ivancev-Tumbas, R. Hobby, B. Kuchle, S. Panglisch, R. Gimbel, p-Nitrophenol removal by combination of powdered activated carbon adsorption and ultrafiltration - comparison of different operational modes. *Water Res.* **42**(15), 4117–4124 (2008)
14. X. Gu, H. Kang, H. Li, X. Liu, F. Dong, M. Fu, J. Chen, Adsorption removal of various nitrophenols in aqueous solution by aminopropyl-modified mesoporous MCM-48. *J. Chem. Eng. Data* **63**(9), 3606–3614 (2018)
15. P. Laveille, A. Falcimaigne, F. Chamouleau, G. Renard, J. Drone, F. Fajula, S. Pulvin, D. Thomas, C. Bailly, A. Galarneau, Hemoglobin immobilized on mesoporous silica as effective material for the removal of polycyclic aromatic hydrocarbons pollutants from water. *New J. Chem.* **34**(10), 2153–2165 (2010)
16. Y. Liu, W. Zhang, X. Li, X. Le, J. Ma, Catalysis of the hydrodechlorination of 4-chlorophenol and the reduction of 4-nitrophenol by Pd/Fe₃O₄@SiO₂/m-SiO₂. *New J. Chem.* **39**(8), 6474–6481 (2015)
17. S. Sargazi, I. Fatima, M. Hassan Kiani, V. Mohammadzadeh, R. Arshad, M. Bilal, A. Rahdar, A.M. Díez-Pascual, R. Behzadmehr, Fluorescent-based nanosensors for selective detection of a wide range of biological macromolecules: A comprehensive review. *Int. J. Biol. Macromol.* **206**, 115–147 (2022)
18. S. Geng, S.M. Lin, S.G. Liu, N.B. Li, H.Q. Luo, A new fluorescent sensor for detecting p-nitrophenol based on β -cyclodextrin-capped ZnO quantum dots. *RSC Adv.* **6**(89), 86061–86067 (2016)
19. L. Han, S.G. Liu, J.Y. Liang, Y.J. Ju, N.B. Li, H.Q. Luo, pH-mediated reversible fluorescence nanoswitch based on inner filter effect induced fluorescence quenching for selective and visual detection of 4-nitrophenol. *J. Hazard. Mater.* **362**, 45–52 (2019)
20. M. Ahmaruzzaman, S. Laxmi, Gayatri, Batch adsorption of 4-nitrophenol by acid activated jute stick char: equilibrium, kinetic and thermodynamic studies. *Chem. Eng. J.* **158**(2), 173–180 (2010)
21. J. Yu, X. Wang, Q. Kang, J. Li, D. Shen, L. Chen, One-pot synthesis of a quantum dot-based molecular imprinting nanosensor for highly selective and sensitive fluorescence detection of

- 4-nitrophenol in environmental waters. *Environ. Sci. Nano* **4**(2), 493–502 (2017)
22. H. Dai, Z. Deng, Y. Zeng, J. Zhang, Y. Yang, Q. Ma, W. Hu, L. Guo, L. Li, S. Wan, H. Liu, Highly sensitive determination of 4-nitrophenol with coumarin-based fluorescent molecularly imprinted poly (ionic liquid). *J. Hazard. Mater.* **398**, 122854 (2020)
 23. X. Yang, J. Wang, D. Su, Q. Xia, F. Chai, C. Wang, F. Qu, Fluorescent detection of TNT and 4-nitrophenol by BSA Au nanoclusters. *Dalton Trans.* **43**(26), 10057–10063 (2014)
 24. J.-M. Yang, X.-W. Hu, Y.-X. Liu, W. Zhang, Fabrication of a carbon quantum dots-immobilized zirconium-based metal-organic framework composite fluorescence sensor for highly sensitive detection of 4-nitrophenol. *Microporous Mesoporous Mater.* **274**, 149–154 (2019)
 25. T. Shu, J. Wang, X. Lin, Z. Zhou, F. Liang, L. Su, X. Zhang, Dual-emissive gold nanoclusters for label-free and separation-free ratiometric fluorescence sensing of 4-nitrophenol based on the inner filter effect. *J. Mater. Chem. C* **6**(18), 5033–5038 (2018)
 26. Y. Zhou, J. Ding, T. Liang, E.S. Abdel-Halim, L. Jiang, J.-J. Zhu, FITC doped rattle-type silica colloidal particle-based ratiometric fluorescent sensor for biosensing and imaging of superoxide anion. *ACS Appl. Mater. Interfaces* **8**(10), 6423–6430 (2016)
 27. C. Chirocov, A. Spoială, C. Păun, L. Crăciun, D. Ficăi, A. Ficăi, E. Andronescu, C. Turculeț, Mesoporous silica platforms with potential applications in release and adsorption of active agents. *Molecules* **25**(17), 3814 (2020)
 28. S.A. Jadhav, Incredible pace of research on mesoporous silica nanoparticles. *Inorg. Chem. Front.* **1**(10), 735–739 (2014)
 29. S.A. Jadhav, I. Miletto, V. Brunella, D. Scalarone, G. Berlier, Porous silica particles: synthesis, physicochemical characterization and evaluation of suspension stability, physical chemistry. *Indian J.* **12**, 102–112 (2017)
 30. S.A. Jadhav, V.S. Patil, P.S. Shinde, S.S. Thoravat, P.S. Patil, A short review on recent progress in mesoporous silicas for the removal of metal ions from water. *Chem. Pap.* **74**(12), 4143–4157 (2020)
 31. S. Nasreen, U. Rafique, S. Ehrman, M.A. Ashraf, Hybrid mesoporous silicates: a distinct aspect to synthesis and application for decontamination of phenols. *Saudi J. Biol. Sci.* **26**(6), 1161–1170 (2019)
 32. S.A. Jadhav, H.B. Garud, A.H. Patil, G.D. Patil, C.R. Patil, T.D. Dongale, P.S. Patil, Recent advancements in silica nanoparticles based technologies for removal of dyes from water. *Coll. Interface Sci. Commun.* **30**, 100181 (2019)
 33. P.S. Shinde, P.S. Suryawanshi, K.K. Patil, V.M. Belekar, S.A. Sankpal, S.D. Delekar, S.A. Jadhav, A brief overview of recent progress in porous silica as catalyst supports. *J. Compos. Sci.* **5**(3), 75 (2021)
 34. C.C. Costa, D. Melo, M.A.F. Melo, M.E. Mendoza, J.C. Nascimento, J.M. Andrade, J.M.F. Barros, Effects of different structure-directing agents (SDA) in MCM-41 on the adsorption of CO₂. *J. Porous Mater.* **21**, 1069–1077 (2014)
 35. P. Horcajada, A. Rámila, J. Pérez-Pariente, M. Vallet-Regí, Influence of pore size of MCM-41 matrices on drug delivery rate. *Microporous Mesoporous Mater.* **68**(1), 105–109 (2004)
 36. M. Vallet-Regí, A. Rámila, R.P. del Real, J. Pérez-Pariente, A new property of MCM-41: drug delivery system. *Chem. Mater.* **13**(2), 308–311 (2001)
 37. H.-T. Fan, X.-G. Liu, X.-J. Xing, B. Li, K. Wang, S.-T. Chen, Z. Wu, D.-F. Qiu, Ordered mesoporous silica cubic particles decorated with silver nanoparticles: a highly active and recyclable heterogeneous catalyst for the reduction of 4-nitrophenol. *Dalton Trans.* **48**(8), 2692–2700 (2019)
 38. M.A. Jalani, L. Yuliani, S.L. Lee, H.O. Lintang, Highly ordered mesoporous silica film nanocomposites containing gold nanoparticles for the catalytic reduction of 4-nitrophenol. *Beilstein J. Nanotechnol.* **10**, 1368–1379 (2019)
 39. L. Tang, J. Tang, G. Zeng, G. Yang, X. Xie, Y. Zhou, Y. Pang, Y. Fang, J. Wang, W. Xiong, Rapid reductive degradation of aqueous p-nitrophenol using nanoscale zero-valent iron particles immobilized on mesoporous silica with enhanced antioxidation effect. *Appl. Surf. Sci.* **333**, 220–228 (2015)
 40. S. Noreen, A. Maqbool, I. Maqbool, A. Shafique, M.M. Khan, Y. Junejo, B. Ahmed, M. Anwar, A. Majeed, M. Abbas, M. Naveed, A. Madni, Multifunctional mesoporous silica-based nanocomposites: Synthesis and biomedical applications. *Mater. Chem. Phys.* **285**, 126132 (2022)
 41. C. Xu, Y. Niu, A. Papat, S. Jambhrunkar, S. Karmakar, C. Yu, Rod-like mesoporous silica nanoparticles with rough surfaces for enhanced cellular delivery. *J. Mater. Chem. B* **2**(3), 253–256 (2014)
 42. N. Mai, L. Danh, H. Dang, H. Nguyen, H. Ta, T. Doan, T. Le, T. Phan, Study on adenosine loading capacity of porous nanosilica for application in drug delivery. *Sci. Technol. Develop. J. Nat. Sci.* **5**(1), 933–41 (2020)
 43. M. Manzano, V. Aina, C.O. Areán, F. Balas, V. Cauda, M. Colilla, M.R. Delgado, Vallet-regí, studies on MCM-41 mesoporous silica for drug delivery: effect of particle morphology and amine functionalization. *Chem. Eng. J.* **137**(1), 30–37 (2008)
 44. P.D.K.P. Ananda, A. Tillekaratne, C. Hettiarachchi, N. Lalichchandran, Sensitive detection of E. coli using bioconjugated fluorescent silica nanoparticles. *Appl. Surf. Sci. Adv.* **6**, 100159 (2021)
 45. Y. Li, Y. Fu, H. Zhang, J. Song, S. Yang, FITC-labeled alendronate as an in vivo bone pH sensor. *Biomed. Res. Int.* **2020**, 4012194 (2020)
 46. N.X.D. Mai, T.-H.T. Nguyen, L.B. Vong, M.-H.D. Dang, T.T.T. Nguyen, L.H.T. Nguyen, H.K.T. Ta, T.-H. Nguyen, T.B. Phan, T.L.H. Doan, Tailoring chemical compositions of biodegradable mesoporous organosilica nanoparticles for controlled slow release of chemotherapeutic drug. *Mater. Sci. Eng. C* **127**, 112232 (2021)
 47. M.F. Villegas, L. Garcia-Uriostegui, O. Rodríguez, I. Izquierdo-Barba, A.J. Salinas, G. Toriz, M. Vallet-Regí, Delgado, lysine-grafted MCM-41 silica as an antibacterial biomaterial. *Bioengineering* **4**(4), 80 (2017)
 48. S. Devi, R. Kaur, B. Singh, A.K. Paul, S. Tyagi, Fluorescent sensing assay for trinitrotoluene using fluorescein isothiocyanate conjugated mesoporous MCM-41 particles. *J. Nanosci. Nanotechnol.* **18**(10), 6838–6849 (2018)
 49. N. Rahman, H. Md Rasid, H. Hassan, M.N. Jalil, Synthesis and characterization of mesoporous silica MCM-41 and SBA-15 from power plant bottom ash. *Malaysian J. Anal. Sci.* **20**, 539–545 (2016)
 50. Y.T. Dang, M.-H. Dinh Dang, N.X. Dat Mai, L.H. Thuy Nguyen, T.B. Phan, H.V. Le, T. Le, Hoang Doan, Room temperature synthesis of biocompatible nano zn-mof for the rapid and selective adsorption of curcumin. *J. Science: Adv. Mater. Devices* **5**, 560–565 (2020)
 51. W.-S. Zou, Y.-Q. Wang, F. Wang, Q. Shao, J. Zhang, J. Liu, Selective fluorescence response and magnetic separation probe for 2,4,6-trinitrotoluene based on iron oxide magnetic nanoparticles. *Anal. Bioanal. Chem* **405**(14), 4905–4912 (2013)

Publisher's Note Springer Nature remains neutral with regard to jurisdictional claims in published maps and institutional affiliations.

Springer Nature or its licensor (e.g. a society or other partner) holds exclusive rights to this article under a publishing agreement with the author(s) or other rightsholder(s); author self-archiving of the accepted manuscript version of this article is solely governed by the terms of such publishing agreement and applicable law.